

Observation of the $Y(4220)$ and $Y(4390)$ in the process $e^+e^- \rightarrow \eta J/\psi$

M. Ablikim,¹ M. N. Achasov,^{10,c} P. Adlarson,⁶⁴ S. Ahmed,¹⁵ M. Albrecht,⁴ A. Amoroso,^{63a,63c} Q. An,^{60,48} Anita,²¹ Y. Bai,⁴⁷ O. Bakina,²⁹ R. Baldini Ferroli,^{23a} I. Balossino,^{24a} Y. Ban,^{38,k} K. Begzsuren,²⁶ J. V. Bennett,⁵ N. Berger,²⁸ M. Bertani,^{23a} D. Bettoni,^{24a} F. Bianchi,^{63a,63c} J. Biernat,⁶⁴ J. Bloms,⁵⁷ A. Bortone,^{63a,63c} I. Boyko,²⁹ R. A. Briere,⁵ H. Cai,⁶⁵ X. Cai,^{1,48} A. Calcaterra,^{23a} G. F. Cao,^{1,52} N. Cao,^{1,52} S. A. Cetin,^{51b} J. F. Chang,^{1,48} W. L. Chang,^{1,52} G. Chelkov,^{29,b} D. Y. Chen,⁶ G. Chen,¹ H. S. Chen,^{1,52} M. L. Chen,^{1,48} S. J. Chen,³⁶ X. R. Chen,²⁵ Y. B. Chen,^{1,48} W. S. Cheng,^{63c} G. Cibinetto,^{24a} F. Cossio,^{63c} X. F. Cui,³⁷ H. L. Dai,^{1,48} J. P. Dai,^{42,g} X. C. Dai,^{1,52} A. Dbeyssi,¹⁵ R. B. de Boer,⁴ D. Dedovich,²⁹ Z. Y. Deng,¹ A. Denig,²⁸ I. Denysenko,²⁹ M. Destefanis,^{63a,63c} F. De Mori,^{63a,63c} Y. Ding,³⁴ C. Dong,³⁷ J. Dong,^{1,48} L. Y. Dong,^{1,52} M. Y. Dong,^{1,48,52} S. X. Du,⁶⁸ J. Fang,^{1,48} S. S. Fang,^{1,52} Y. Fang,¹ R. Farinelli,^{24a} L. Fava,^{63b,63c} F. Feldbauer,⁴ G. Felici,^{23a} C. Q. Feng,^{60,48} M. Fritsch,⁴ C. D. Fu,¹ Y. Fu,¹ X. L. Gao,^{60,48} Y. Gao,⁶¹ Y. Gao,^{38,k} Y. G. Gao,⁶ I. Garzia,^{24a,24b} E. M. Gersabeck,⁵⁵ A. Gilman,⁵⁶ K. Goetzen,¹¹ L. Gong,³⁷ W. X. Gong,^{1,48} W. Gradl,²⁸ M. Greco,^{63a,63c} L. M. Gu,³⁶ M. H. Gu,^{1,48} S. Gu,² Y. T. Gu,¹³ C. Y. Guan,^{1,52} A. Q. Guo,²² L. B. Guo,³⁵ R. P. Guo,⁴⁰ Y. P. Guo,²⁸ Y. P. Guo,^{9,h} A. Guskov,²⁹ S. Han,⁶⁵ T. T. Han,⁴¹ T. Z. Han,^{9,h} X. Q. Hao,¹⁶ F. A. Harris,⁵³ K. L. He,^{1,52} F. H. Heinsius,⁴ T. Held,⁴ Y. K. Heng,^{1,48,52} M. Himmelreich,^{11,f} T. Holtmann,⁴ Y. R. Hou,⁵² Z. L. Hou,¹ H. M. Hu,^{1,52} J. F. Hu,^{42,g} T. Hu,^{1,48,52} Y. Hu,¹ G. S. Huang,^{60,48} L. Q. Huang,⁶¹ X. T. Huang,⁴¹ Z. Huang,^{38,k} N. Huesken,⁵⁷ T. Hussain,⁶² W. Ikegami Andersson,⁶⁴ W. Imoehl,²² M. Irshad,^{60,48} S. Jaeger,⁴ S. Janchiv,^{26,j} Q. Ji,¹ Q. P. Ji,¹⁶ X. B. Ji,^{1,52} X. L. Ji,^{1,48} H. B. Jiang,⁴¹ X. S. Jiang,^{1,48,52} X. Y. Jiang,³⁷ J. B. Jiao,⁴¹ Z. Jiao,¹⁸ S. Jin,³⁶ Y. Jin,⁵⁴ T. Johansson,⁶⁴ N. Kalantar-Nayestanaki,³¹ X. S. Kang,³⁴ R. Kappert,³¹ M. Kavatsyuk,³¹ B. C. Ke,^{43,i} I. K. Keshk,⁴ A. Khoukaz,⁵⁷ P. Kiese,²⁸ R. Kiuchi,¹ R. Kliemt,¹¹ L. Koch,³⁰ O. B. Kolcu,^{51b,c} B. Kopf,⁴ M. Kuemmel,⁴ M. Kuessner,⁴ A. Kupsc,⁶⁴ M. G. Kurth,^{1,52} W. Kühn,³⁰ J. J. Lane,⁵⁵ J. S. Lange,³⁰ P. Larin,¹⁵ L. Lavezzi,^{63c} H. Leithoff,²⁸ M. Lellmann,²⁸ T. Lenz,²⁸ C. Li,³⁹ C. H. Li,³³ Cheng Li,^{60,48} D. M. Li,⁶⁸ F. Li,^{1,48} G. Li,¹ H. B. Li,^{1,52} H. J. Li,^{9,h} J. L. Li,⁴¹ J. Q. Li,⁴ Ke Li,¹ L. K. Li,¹ Lei Li,³ P. L. Li,^{60,48} P. R. Li,³² S. Y. Li,⁵⁰ W. D. Li,^{1,52} W. G. Li,¹ X. H. Li,^{60,48} X. L. Li,⁴¹ Z. B. Li,⁴⁹ Z. Y. Li,⁴⁹ H. Liang,^{60,48} H. Liang,^{1,52} Y. F. Liang,⁴⁵ Y. T. Liang,²⁵ L. Z. Liao,^{1,52} J. Libby,²¹ C. X. Lin,⁴⁹ B. Liu,^{42,g} B. J. Liu,¹ C. X. Liu,¹ D. Liu,^{60,48} D. Y. Liu,^{42,g} F. H. Liu,⁴⁴ Fang Liu,¹ Feng Liu,⁶ H. B. Liu,¹³ H. M. Liu,^{1,52} Huanhuan Liu,¹ Huihui Liu,¹⁷ J. B. Liu,^{60,48} J. Y. Liu,^{1,52} K. Liu,¹ K. Y. Liu,³⁴ Ke Liu,⁶ L. Liu,^{60,48} Q. Liu,⁵² S. B. Liu,^{60,48} Shuai Liu,⁴⁶ T. Liu,^{1,52} X. Liu,³² Y. B. Liu,³⁷ Z. A. Liu,^{1,48,52} Z. Q. Liu,⁴¹ Y. F. Long,^{38,k} X. C. Lou,^{1,48,52} F. X. Lu,¹⁶ H. J. Lu,¹⁸ J. D. Lu,^{1,52} J. G. Lu,^{1,48} X. L. Lu,¹ Y. Lu,¹ Y. P. Lu,^{1,48} C. L. Luo,³⁵ M. X. Luo,⁶⁷ P. W. Luo,⁴⁹ T. Luo,^{9,h} X. L. Luo,^{1,48} S. Lusso,^{63c} X. R. Lyu,⁵² F. C. Ma,³⁴ H. L. Ma,¹ L. L. Ma,⁴¹ M. M. Ma,^{1,52} Q. M. Ma,¹ R. Q. Ma,^{1,52} R. T. Ma,⁵² X. N. Ma,³⁷ X. X. Ma,^{1,52} X. Y. Ma,^{1,48} Y. M. Ma,⁴¹ F. E. Maas,¹⁵ M. Maggiora,^{63a,63c} S. Maldaner,²⁸ S. Malde,⁵⁸ Q. A. Malik,⁶² A. Mangoni,^{23b} Y. J. Mao,^{38,k} Z. P. Mao,¹ S. Marcello,^{63a,63c} Z. X. Meng,⁵⁴ J. G. Messchendorp,³¹ G. Mezzadri,^{24a} T. J. Min,³⁶ R. E. Mitchell,²² X. H. Mo,^{1,48,52} Y. J. Mo,⁶ N. Yu. Muchnoi,^{10,c} H. Muramatsu,⁵⁶ S. Nakhoul,^{11,f} Y. Nefedov,²⁹ F. Nerling,^{11,f} I. B. Nikolaev,^{10,c} Z. Ning,^{1,48} S. Nisar,^{8,i} S. L. Olsen,⁵² Q. Ouyang,^{1,48,52} S. Pacetti,^{23b} X. Pan,⁴⁶ Y. Pan,⁵⁵ A. Pathak,¹ P. Patteri,^{23a} M. Pelizaeus,⁴ H. P. Peng,^{60,48} K. Peters,^{11,f} J. Pettersson,⁶⁴ J. L. Ping,³⁵ R. G. Ping,^{1,52} A. Pitka,⁴ R. Poling,⁵⁶ V. Prasad,^{60,48} H. Qi,^{60,48} H. R. Qi,⁵⁰ M. Qi,³⁶ T. Y. Qi,² S. Qian,^{1,48} W.-B. Qian,⁵² Z. Qian,⁴⁹ C. F. Qiao,⁵² L. Q. Qin,¹² X. P. Qin,¹³ X. S. Qin,⁴ Z. H. Qin,^{1,48} J. F. Qiu,¹ S. Q. Qu,³⁷ K. H. Rashid,⁶² K. Ravindran,²¹ C. F. Redmer,²⁸ A. Rivetti,^{63c} V. Rodin,³¹ M. Rolo,^{63c} G. Rong,^{1,52} Ch. Rosner,¹⁵ M. Rump,⁵⁷ A. Sarantsev,^{29,d} Y. Schelhaas,²⁸ C. Schnier,⁴ K. Schoenning,⁶⁴ D. C. Shan,⁴⁶ W. Shan,¹⁹ X. Y. Shan,^{60,48} M. Shao,^{60,48} C. P. Shen,² P. X. Shen,³⁷ X. Y. Shen,^{1,52} H. C. Shi,^{60,48} R. S. Shi,^{1,52} X. Shi,^{1,48} X. D. Shi,^{60,48} J. J. Song,⁴¹ Q. Q. Song,^{60,48} W. M. Song,²⁷ Y. X. Song,^{38,k} S. Sosio,^{63a,63c} S. Spataro,^{63a,63c} F. F. Sui,⁴¹ G. X. Sun,¹ J. F. Sun,¹⁶ L. Sun,⁶⁵ S. S. Sun,^{1,52} T. Sun,^{1,52} W. Y. Sun,³⁵ Y. J. Sun,^{60,48} Y. K. Sun,^{60,48} Y. Z. Sun,¹ Z. T. Sun,¹ Y. H. Tan,⁶⁵ Y. X. Tan,^{60,48} C. J. Tang,⁴⁵ G. Y. Tang,¹ J. Tang,⁴⁹ V. Thoren,⁶⁴ B. Tsednee,²⁶ I. Uman,^{51d} B. Wang,¹ B. L. Wang,⁵² C. W. Wang,³⁶ D. Y. Wang,^{38,k} H. P. Wang,^{1,52} K. Wang,^{1,48} L. L. Wang,¹ M. Wang,⁴¹ M. Z. Wang,^{38,k} Meng Wang,^{1,52} W. H. Wang,⁶⁵ W. P. Wang,^{60,48} X. Wang,^{38,k} X. F. Wang,³² X. L. Wang,^{9,h} Y. Wang,⁴⁹ Y. Wang,^{60,48} Y. D. Wang,¹⁵ Y. F. Wang,^{1,48,52} Y. Q. Wang,¹ Z. Wang,^{1,48} Z. Y. Wang,¹ Ziyi Wang,⁵² Zongyuan Wang,^{1,52} T. Weber,⁴ D. H. Wei,¹² P. Weidenkaff,²⁸ F. Weidner,⁵⁷ S. P. Wen,¹ D. J. White,⁵⁵ U. Wiedner,⁴ G. Wilkinson,⁵⁸ M. Wolke,⁶⁴ L. Wollenberg,⁴ J. F. Wu,^{1,52} L. H. Wu,¹ L. J. Wu,^{1,52} X. Wu,^{9,h} Z. Wu,^{1,48} L. Xia,^{60,48} H. Xiao,^{9,h} S. Y. Xiao,¹ Y. J. Xiao,^{1,52} Z. J. Xiao,³⁵ X. H. Xie,^{38,k} Y. G. Xie,^{1,48} Y. H. Xie,⁶ T. Y. Xing,^{1,52} X. A. Xiong,^{1,52} G. F. Xu,¹ J. J. Xu,³⁶ Q. J. Xu,¹⁴ W. Xu,^{1,52} X. P. Xu,⁴⁶ L. Yan,^{63a,63c} L. Yan,^{9,h} W. B. Yan,^{60,48} W. C. Yan,⁶⁸ Xu Yan,⁴⁶ H. J. Yang,^{42,g} H. X. Yang,¹ L. Yang,⁶⁵ R. X. Yang,^{60,48} S. L. Yang,^{1,52} Y. H. Yang,³⁶ Y. X. Yang,¹² Yifan Yang,^{1,52} Zhi Yang,²⁵ M. Ye,^{1,48} M. H. Ye,⁷ J. H. Yin,¹ Z. Y. You,⁴⁹ B. X. Yu,^{1,48,52} C. X. Yu,³⁷ G. Yu,^{1,52} J. S. Yu,^{20,l} T. Yu,⁶¹ C. Z. Yuan,^{1,52} W. Yuan,^{63a,63c} X. Q. Yuan,^{38,k} Y. Yuan,¹ Z. Y. Yuan,⁴⁹ C. X. Yue,³³ A. Yuncu,^{51b,a} A. A. Zafar,⁶² Y. Zeng,^{20,l} B. X. Zhang,¹ Guangyi Zhang,¹⁶ H. H. Zhang,⁴⁹ H. Y. Zhang,^{1,48} J. L. Zhang,⁶⁶ J. Q. Zhang,⁴ J. W. Zhang,^{1,48,52} J. Y. Zhang,¹ J. Z. Zhang,^{1,52} Jianyu Zhang,^{1,52} Jiawei Zhang,^{1,52} L. Zhang,¹ Lei Zhang,³⁶ S. Zhang,⁴⁹ S. F. Zhang,³⁶ T. J. Zhang,^{42,g} X. Y. Zhang,⁴¹ Y. Zhang,⁵⁸

Y. H. Zhang,^{1,48} Y. T. Zhang,^{60,48,*} Yan Zhang,^{60,48} Yao Zhang,¹ Yi Zhang,^{9,h} Z. H. Zhang,⁶ Z. Y. Zhang,⁶⁵ G. Zhao,¹ J. Zhao,³³ J. Y. Zhao,^{1,52} J. Z. Zhao,^{1,48} Lei Zhao,^{60,48} Ling Zhao,¹ M. G. Zhao,³⁷ Q. Zhao,¹ S. J. Zhao,⁶⁸ Y. B. Zhao,^{1,48} Y. X. Zhao,²⁵ Z. G. Zhao,^{60,48} A. Zhemchugov,^{29,b} B. Zheng,⁶¹ J. P. Zheng,^{1,48} Y. Zheng,^{38,k} Y. H. Zheng,⁵² B. Zhong,³⁵ C. Zhong,⁶¹ L. P. Zhou,^{1,52} Q. Zhou,^{1,52} X. Zhou,⁶⁵ X. K. Zhou,⁵² X. R. Zhou,^{60,48} A. N. Zhu,^{1,52} J. Zhu,³⁷ K. Zhu,¹ K. J. Zhu,^{1,48,52} S. H. Zhu,⁵⁹ W. J. Zhu,³⁷ X. L. Zhu,⁵⁰ Y. C. Zhu,^{60,48} Z. A. Zhu,^{1,52} B. S. Zou,¹ and J. H. Zou¹

(BESIII Collaboration)

- ¹*Institute of High Energy Physics, Beijing 100049, People's Republic of China*
²*Beihang University, Beijing 100191, People's Republic of China*
³*Beijing Institute of Petrochemical Technology, Beijing 102617, People's Republic of China*
⁴*Bochum Ruhr-University, D-44780 Bochum, Germany*
⁵*Carnegie Mellon University, Pittsburgh, Pennsylvania 15213, USA*
⁶*Central China Normal University, Wuhan 430079, People's Republic of China*
⁷*China Center of Advanced Science and Technology, Beijing 100190, People's Republic of China*
⁸*COMSATS University Islamabad, Lahore Campus, Defence Road, Off Raiwind Road, 54000 Lahore, Pakistan*
⁹*Fudan University, Shanghai 200443, People's Republic of China*
¹⁰*G.I. Budker Institute of Nuclear Physics SB RAS (BINP), Novosibirsk 630090, Russia*
¹¹*GSI Helmholtzcentre for Heavy Ion Research GmbH, D-64291 Darmstadt, Germany*
¹²*Guangxi Normal University, Guilin 541004, People's Republic of China*
¹³*Guangxi University, Nanning 530004, People's Republic of China*
¹⁴*Hangzhou Normal University, Hangzhou 310036, People's Republic of China*
¹⁵*Helmholtz Institute Mainz, Johann-Joachim-Becher-Weg 45, D-55099 Mainz, Germany*
¹⁶*Henan Normal University, Xinxiang 453007, People's Republic of China*
¹⁷*Henan University of Science and Technology, Luoyang 471003, People's Republic of China*
¹⁸*Huangshan College, Huangshan 245000, People's Republic of China*
¹⁹*Hunan Normal University, Changsha 410081, People's Republic of China*
²⁰*Hunan University, Changsha 410082, People's Republic of China*
²¹*Indian Institute of Technology Madras, Chennai 600036, India*
²²*Indiana University, Bloomington, Indiana 47405, USA*
^{23a}*INFN Laboratori Nazionali di Frascati, I-00044, Frascati, Italy*
^{23b}*INFN and University of Perugia, I-06100, Perugia, Italy*
^{24a}*INFN Sezione di Ferrara, I-44122, Ferrara, Italy*
^{24b}*University of Ferrara, I-44122, Ferrara, Italy*
²⁵*Institute of Modern Physics, Lanzhou 730000, People's Republic of China*
²⁶*Institute of Physics and Technology, Peace Ave. 54B, Ulaanbaatar 13330, Mongolia*
²⁷*Jilin University, Changchun 130012, People's Republic of China*
²⁸*Johannes Gutenberg University of Mainz, Johann-Joachim-Becher-Weg 45, D-55099 Mainz, Germany*
²⁹*Joint Institute for Nuclear Research, 141980 Dubna, Moscow region, Russia*
³⁰*Justus-Liebig-Universitaet Giessen, II. Physikalisches Institut, Heinrich-Buff-Ring 16, D-35392 Giessen, Germany*
³¹*KVI-CART, University of Groningen, NL-9747 AA Groningen, The Netherlands*
³²*Lanzhou University, Lanzhou 730000, People's Republic of China*
³³*Liaoning Normal University, Dalian 116029, People's Republic of China*
³⁴*Liaoning University, Shenyang 110036, People's Republic of China*
³⁵*Nanjing Normal University, Nanjing 210023, People's Republic of China*
³⁶*Nanjing University, Nanjing 210093, People's Republic of China*
³⁷*Nankai University, Tianjin 300071, People's Republic of China*
³⁸*Peking University, Beijing 100871, People's Republic of China*
³⁹*Qufu Normal University, Qufu 273165, People's Republic of China*
⁴⁰*Shandong Normal University, Jinan 250014, People's Republic of China*
⁴¹*Shandong University, Jinan 250100, People's Republic of China*
⁴²*Shanghai Jiao Tong University, Shanghai 200240, People's Republic of China*
⁴³*Shanxi Normal University, Linfen 041004, People's Republic of China*
⁴⁴*Shanxi University, Taiyuan 030006, People's Republic of China*
⁴⁵*Sichuan University, Chengdu 610064, People's Republic of China*
⁴⁶*Soochow University, Suzhou 215006, People's Republic of China*
⁴⁷*Southeast University, Nanjing 211100, People's Republic of China*

- ⁴⁸State Key Laboratory of Particle Detection and Electronics, Beijing 100049, Hefei 230026, People's Republic of China
- ⁴⁹Sun Yat-Sen University, Guangzhou 510275, People's Republic of China
- ⁵⁰Tsinghua University, Beijing 100084, People's Republic of China
- ^{51a}Ankara University, 06100 Tandogan, Ankara, Turkey
- ^{51b}Istanbul Bilgi University, 34060 Eyup, Istanbul, Turkey
- ^{51c}Uludag University, 16059 Bursa, Turkey
- ^{51d}Near East University, Nicosia, North Cyprus, Mersin 10, Turkey
- ⁵²University of Chinese Academy of Sciences, Beijing 100049, People's Republic of China
- ⁵³University of Hawaii, Honolulu, Hawaii 96822, USA
- ⁵⁴University of Jinan, Jinan 250022, People's Republic of China
- ⁵⁵University of Manchester, Oxford Road, Manchester, M13 9PL, United Kingdom
- ⁵⁶University of Minnesota, Minneapolis, Minnesota 55455, USA
- ⁵⁷University of Muenster, Wilhelm-Klemm-Str. 9, 48149 Muenster, Germany
- ⁵⁸University of Oxford, Keble Rd, Oxford, UK OX13RH
- ⁵⁹University of Science and Technology Liaoning, Anshan 114051, People's Republic of China
- ⁶⁰University of Science and Technology of China, Hefei 230026, People's Republic of China
- ⁶¹University of South China, Hengyang 421001, People's Republic of China
- ⁶²University of the Punjab, Lahore-54590, Pakistan
- ^{63a}University of Turin, I-10125, Turin, Italy
- ^{63b}University of Eastern Piedmont, I-15121, Alessandria, Italy
- ^{63c}INFN, I-10125, Turin, Italy
- ⁶⁴Uppsala University, Box 516, SE-75120 Uppsala, Sweden
- ⁶⁵Wuhan University, Wuhan 430072, People's Republic of China
- ⁶⁶Xinyang Normal University, Xinyang 464000, People's Republic of China
- ⁶⁷Zhejiang University, Hangzhou 310027, People's Republic of China
- ⁶⁸Zhengzhou University, Zhengzhou 450001, People's Republic of China



(Received 9 March 2020; revised 20 April 2020; accepted 24 July 2020; published 24 August 2020)

The cross sections of the process $e^+e^- \rightarrow \eta J/\psi$ at center-of-mass energies (\sqrt{s}) between 3.81 and 4.60 GeV are measured with high precision by using data samples collected with the BESIII detector operating at the BEPCII storage ring. Three structures are observed by analyzing the line shape of the measured cross sections, and a maximum-likelihood fit including three resonances is performed by assuming the lowest lying structure is the $\psi(4040)$. For the other resonances, we obtain masses of $(4218.6 \pm 3.8 \pm 2.5)$ and $(4382.0 \pm 13.3 \pm 1.7)$ MeV/ c^2 with corresponding widths of $(82.0 \pm 5.7 \pm 0.4)$ and $(135.8 \pm 60.8 \pm 22.5)$ MeV, respectively, where the first uncertainties are statistical and the second ones systematic. The measured resonant parameters are consistent with those of the $Y(4220)$ and $Y(4390)$ from previous measurements of different final states. For the first time, we observe the decays of the $Y(4220)$ and $Y(4390)$ into $\eta J/\psi$ final states.

DOI: [10.1103/PhysRevD.102.031101](https://doi.org/10.1103/PhysRevD.102.031101)

^aAlso at Bogazici University, 34342 Istanbul, Turkey.

^bAlso at the Moscow Institute of Physics and Technology, Moscow 141700, Russia.

^cAlso at the Novosibirsk State University, Novosibirsk, 630090, Russia.

^dAlso at the NRC “Kurchatov Institute”, PNPI, 188300, Gatchina, Russia.

^eAlso at Istanbul Arel University, 34295 Istanbul, Turkey.

^fAlso at Goethe University Frankfurt, 60323 Frankfurt am Main, Germany.

^gAlso at Key Laboratory for Particle Physics, Astrophysics and Cosmology, Ministry of Education; Shanghai Key Laboratory for Particle Physics and Cosmology; Institute of Nuclear and Particle Physics, Shanghai 200240, People's Republic of China.

^hAlso at Key Laboratory of Nuclear Physics and Ion-beam Application (MOE) and Institute of Modern Physics, Fudan University, Shanghai 200443, People's Republic of China.

ⁱAlso at Harvard University, Department of Physics, Cambridge, Massachusetts 02138, USA.

^jCurrently at: Institute of Physics and Technology, Peace Ave.54B, Ulaanbaatar 13330, Mongolia.

^kAlso at State Key Laboratory of Nuclear Physics and Technology, Peking University, Beijing 100871, People's Republic of China.

^lSchool of Physics and Electronics, Hunan University, Changsha 410082, China.

*zhangyt2017@ustc.edu.cn

In the past decades, a series of charmoniumlike states with $J^{PC} = 1^{--}$, so-called Y states, were observed in e^+e^- annihilation experiments. Besides three well-established charmonium states observed in the inclusive hadronic cross section [1], i.e., $\psi(4040)$, $\psi(4160)$, and $\psi(4415)$, four additional states, i.e., $Y(4008)$, $Y(4260)$, $Y(4360)$ and $Y(4660)$, were reported in the initial-state radiation (ISR) processes $e^+e^- \rightarrow \gamma_{ISR}\pi^+\pi^-\psi$ at the B factories [2–9] and (or) in the direct production processes $e^+e^- \rightarrow \pi^+\pi^-\psi$ at the CLEO and BESIII experiments [10,11], where the symbol ψ represents both J/ψ and $\psi(3686)$ vector charmonium states below the open-charm production threshold. The latest results of the BESIII experiment for $e^+e^- \rightarrow \pi^+\pi^-J/\psi$ show that the $Y(4260)$ may consist of two components, i.e., $Y(4220)$ and $Y(4320)$ [12]. Dedicated measurements by BESIII of the cross sections for $e^+e^- \rightarrow \pi^+\pi^-\psi(3686)$ [13], $e^+e^- \rightarrow \pi^+\pi^-h_c$ [14], $\omega\chi_{c0}$ [15] and $\pi^+D^0D^{*-}$ [16] also support the existence of structures at 4220 MeV/ c^2 . A higher mass state, $Y(4390)$, is also observed in the processes $e^+e^- \rightarrow \pi^+\pi^-\psi(3686)$ [13] and $e^+e^- \rightarrow \pi^+\pi^-h_c$ [14], which do not match any known vector charmonium or charmoniumlike states. Up to now, the internal structure of these Y states are unclear and many theoretical models, such as hybrid charmonium, tetraquark or hadronic molecule, are proposed to interpret their natures, but none of them are conclusive [17]. Comprehensive measurements of the resonant parameters of the Y states will provide further insights into their internal structures. To understand the internal structure of Y states, it is advantageous to study their hadronic transitions to the lightest charmonium states [18–22]. From a theoretical point of view, the amplitude of two-body decays, e.g., $e^+e^- \rightarrow \eta J/\psi$, can be calculated relatively easier than those of three-body processes. For example, theoretical approaches that incorporate meson-loop mechanisms [23–26] for two-body decays are regarded as sensitive probes to distinguish conventional vector charmonium states from exotic ones, in particular, with respect to the hadronic molecule case. In addition, two-body decay processes provide a rigorous test of open-charm effects and help us to understand nonperturbative QCD effects in the charmonium-mass region [27].

The process $e^+e^- \rightarrow \eta J/\psi$ was studied using ISR by Belle [28]. Unlike the process $e^+e^- \rightarrow \pi^+\pi^-J/\psi$ [12], two resonant structures at 4040 and 4160 MeV/ c^2 , regarded as the $\psi(4040)$ and $\psi(4160)$, respectively, were observed by studying the cross section dependence on the center-of-mass (c.m.) energy. Using data samples at 17 c.m. energies from 3.81 to 4.60 GeV, BESIII reported more accurate measurements of cross sections of the $e^+e^- \rightarrow \eta J/\psi$ process [29]. The BESIII data agree well with that of Belle. However, due to a limited coverage in c.m. energies it was not possible to establish any potential Y states.

In this Letter, we present an updated analysis of $e^+e^- \rightarrow \eta J/\psi$ at c.m. energies between 3.81 and 4.60 GeV, where

the $J/\psi \rightarrow \ell^+\ell^-$ ($\ell = e/\mu$) and $\eta \rightarrow \gamma\gamma$ (model) and $\eta \rightarrow \pi^+\pi^-\pi^0$ (mode II) decay modes are reconstructed. The samples used in this analysis include a set of high luminosity data samples with more than 50 pb $^{-1}$ at each c.m. energy adding up to a total integrated luminosity of 13.1 fb $^{-1}$ (referred to as “XYZ data”) [30]. Compared to the previous analysis [29], 10 high luminosity datasets [30], which are of integrated luminosity greater than 5 fb $^{-1}$ with c.m. energies around 4200 MeV/ c^2 , are added. A set of data samples of about 7–9 pb $^{-1}$ at each c.m. energy with a total integrated luminosity of 0.8 fb $^{-1}$ (named as “scan data”) [30] was used in this study, in addition, which is not available in the earlier study of Ref. [29]. The addition of reconstructed $\eta \rightarrow \pi^+\pi^-\pi^0$, which were not used in [29], leads to an increase of 25% in statistics.

Details on the features and capabilities of the BEPCII collider and the BESIII detector can be found in Ref. [31]. The GEANT4-based [32] Monte Carlo (MC) simulation software package BOOST [33], which includes the geometric description of the BESIII detector and the detector response, is used to optimize event selection criteria, determine the detection efficiencies, and estimate the background events. Signal MC samples of $e^+e^- \rightarrow \eta J/\psi$ with the corresponding J/ψ and η decay modes are generated using HELAMP [34] and EVTGEN [35] at each c.m. energy. The ISR is simulated with KKMC [36] by adjusting the maximal energy of the ISR photon according to the $\eta J/\psi$ mass threshold. Final-state radiation (FSR) is simulated with PHOTOS [37]. Possible background contributions are studied with the inclusive MC samples generated by KKMC with comparable luminosity to the XYZ data, where the known decay modes are simulated by EVTGEN [35] with branching fractions taken from the PDG [1], and the remaining unknown are simulated with the LUNDCHARM model [38].

We use the same selection criteria for the charged tracks and photons as described in Ref. [29]. Candidate events are required to have two (mode I) and four (mode II) charged tracks, in each case with zero net charge. Since pions and leptons have distinct momenta for the signal processes, we assign charged tracks with momenta larger than 1.0 GeV/ c to leptons, otherwise they are regarded as pions. The separation of electrons from muons is realized by considering the deposited energy in the electromagnetic calorimeter E . Muon candidates are required to fulfill $E < 0.5$ GeV while electron candidates need to satisfy $E/p > 0.8$, where p is the particle momentum. The signal candidate events are required to contain a pair of leptons with same flavor but opposite charge. In mode II, two additional pions with opposite charge are further required. Candidate events with at least two photons are kept for further analysis.

To improve the kinematic resolution and to suppress the background events, a four-constraint (4C) kinematic fit imposing energy-momentum conservation with the

hypothesis of $e^+e^- \rightarrow \gamma\gamma\ell^+\ell^-$ is applied for the candidates of mode I, while a five-constraint (5C) kinematic fit is performed under the hypothesis of $e^+e^- \rightarrow \gamma\gamma\pi^+\pi^-\ell^+\ell^-$ with an additional π^0 mass constraint for the photon pair in case of mode II. For events with more than two photon candidates, all photon pairs are tested in the kinematic fit and the combination with the smallest $\chi_{4C/5C}^2$ is retained. The surviving events are required to satisfy $\chi_{4C}^2 < 40$ or $\chi_{5C}^2 < 80$. To further suppress the background events from the radiative Bhabha and dimuon events associated with a random photon candidate for events of the mode I, the energy of each of two selected photons is required to be larger than 80 MeV.

Figure 1 presents the distributions of the invariant mass of the $\ell^+\ell^-$ pair ($M(\ell^+\ell^-)$) versus that of the $\gamma\gamma$ pair ($M(\gamma\gamma)$) or $\pi^+\pi^-\pi^0$ combination ($M(\pi^+\pi^-\pi^0)$) for the surviving events at $\sqrt{s} = 4.1780$ GeV after applying all previously described selection criteria. Clear accumulations

of candidate events of the signal process $e^+e^- \rightarrow \eta J/\psi$ are observed around the intersections of the J/ψ and η mass regions. Signal candidates are required to be within the J/ψ mass region, defined as $[3.067, 3.127]$ GeV/ c^2 on the lepton pair invariant mass, which is $\pm 3\sigma$ of corresponding resolution obtained from signal MC simulation. The events in the J/ψ mass sideband regions, defined as $[3.027, 3.057]$ and $[3.137, 3.167]$ GeV/ c^2 , are used to estimate the non- J/ψ background, and non-peaking background are observed in the $M(\gamma\gamma)$ and $M(\pi^+\pi^-\pi^0)$ distributions. A significantly larger non- J/ψ background is observed in the e^+e^- mode than in the $\mu^+\mu^-$ mode in mode I, which is due to the large Bhabha cross section.

The Born cross section is obtained from the formula

$$\sigma^B = \frac{N^{\text{sig}}}{\mathcal{L}_{\text{int}} \cdot (1 + \delta)^r \cdot (1 + \delta)^v \cdot \mathcal{B}r \cdot \epsilon}, \quad (1)$$

where N^{sig} is the signal yield, which will be explained below, \mathcal{L}_{int} is the integrated luminosity, $(1 + \delta)^r$ is the ISR correction factor, $(1 + \delta)^v$ is the vacuum polarization factor taken from a QED calculation [39], $\mathcal{B}r$ is the product of the branching fractions of the subsequent decays of intermediate states quoted from the PDG [1], and ϵ is the detection efficiency obtained from a MC simulation. The ISR correction factor is obtained by using iteratively the QED calculation as described in Ref. [40], where the last measured cross section is taken as the input line shape.

For the XYZ data, an unbinned maximum-likelihood fit is performed on the distributions of $M(\gamma\gamma)$ and $M(\pi^+\pi^-\pi^0)$ to extract the signal yields, where the signal is described by a MC-simulated shape convolved with a Gaussian function, representing the resolution difference between data and MC simulation, and the background is described by a linear function. A simultaneous fit is performed by considering the four processes, i.e., two observation variables $M(\gamma\gamma)$ and $M(\pi^+\pi^-\pi^0)$, as well as two J/ψ decay modes e^+e^- and $\mu^+\mu^-$ for the 27 data samples at different c.m. energies. In the fit, the different processes are constrained by the same Born cross section σ^B , and the expected signal yields are $N^{\text{sig}} = \sigma^B \cdot \mathcal{L}_{\text{int}} \cdot (1 + \delta)^r \cdot (1 + \delta)^v \cdot \mathcal{B}r \cdot \epsilon$. Among the different datasets we used common fit parameters for the mean and width of the Gaussian function representing differences between data and MC. For center-of-mass energies where the signal is not significant, we set the upper limits at the 90% confidence level (C.L.) on the cross sections.

For the scan datasets, the signal yields are determined by counting the number of events in the η signal region $[0.517, 0.547]$ GeV/ c^2 after subtracting the background estimated by the normalized number of events in the J/ψ mass sideband region. In this case, only mode I is considered to extract the Born cross sections by using Eq. (1).

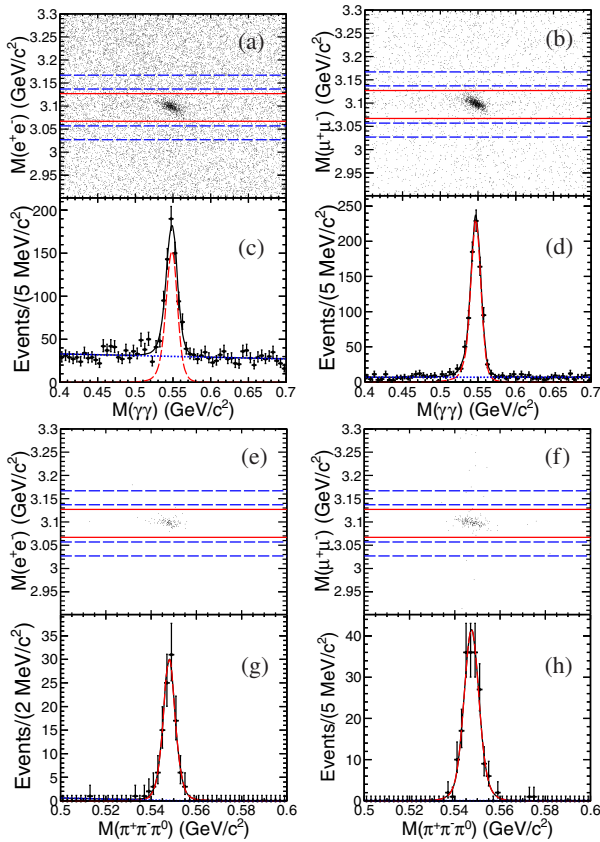


FIG. 1. (a),(b),(e),(f): Cscatter plots of $M(\ell^+\ell^-)$ versus $M(\gamma\gamma/\pi^+\pi^-\pi^0)$. (c),(d),(g),(h): Spectra of the $M(\gamma\gamma/\pi^+\pi^-\pi^0)$ distribution in the J/ψ signal region for data at $\sqrt{s} = 4.1780$ GeV. The upper (lower) 4 panels correspond to the mode I (mode II). In the scatter plots, the solid (red) lines denote the signal region, and the dashed (blue) lines for the sideband region. For the mass spectra plots, the dots with error bars represent data. The solid (black), long-dashed (red) and short-dashed (blue) lines correspond to the fit result, signal and background, respectively.

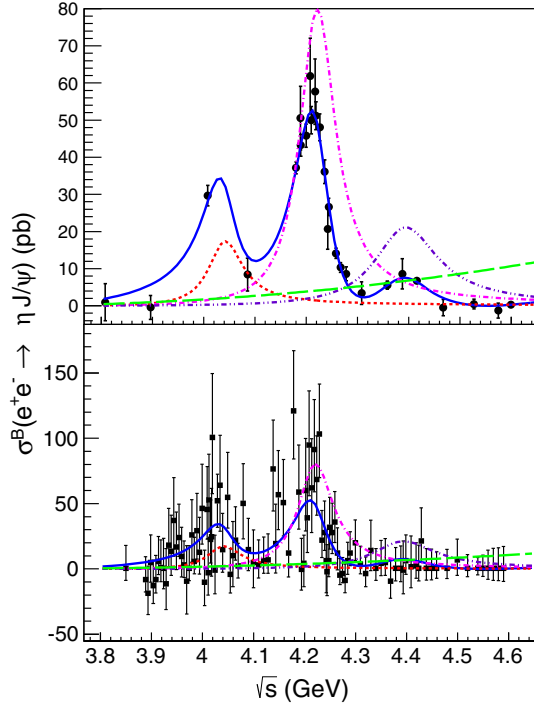


FIG. 2. Top: Cross section and fits of $e^+e^- \rightarrow \eta J/\psi$ for XYZ data. Bottom: Same for the scan data. Dots with error bars are data. The solid (blue) curves represent the fit results of the following interfering amplitudes: $\psi(4040)$ (dashed red), $Y(4220)$ (short-dashed pink), $Y(4390)$ (short-dashed purple), and P-PHSP (long-dashed green).

The measured Born cross sections at the different c.m. energies for both XYZ and scan data are shown in the top and bottom panels of Fig. 2, respectively. Clear structures are observed. The numbers used in the calculation of the Born cross section (upper limit at the 90% C.L.) are summarized in Tables I and II in the Supplemental Material [30].

The following sources of systematic uncertainty are considered in the cross section measurements. The

TABLE I. Fitting results of the $e^+e^- \rightarrow \eta J/\psi$ decay.

Parameters	Solution 1	Solution 2	Solution 3
$M_1(\text{MeV}/c^2)$		4039(fixed)	
$\Gamma_1(\text{MeV})$		80(fixed)	
$\Gamma_1^{e^+e^-} \mathcal{B}r_1$ (eV)	1.5 ± 0.3	1.4 ± 0.3	7.0 ± 0.6
ϕ_1 (rad)	3.3 ± 0.3	3.1 ± 0.3	4.5 ± 0.2
$M_2(\text{MeV}/c^2)$		4218.6 ± 3.8	
$\Gamma_2(\text{MeV})$		82.0 ± 5.7	
$\Gamma_2^{e^+e^-} \mathcal{B}r_2$ (eV)	8.0 ± 1.7	4.8 ± 1.0	7.0 ± 1.5
ϕ_2 (rad)	4.2 ± 0.4	3.6 ± 0.3	2.9 ± 0.3
$M_3(\text{MeV}/c^2)$		4382.0 ± 13.3	
$\Gamma_3(\text{MeV})$		135.8 ± 60.8	
$\Gamma_3^{e^+e^-} \mathcal{B}r_3$ (eV)	3.4 ± 2.2	1.5 ± 1.0	1.7 ± 1.1
ϕ_3 (rad)	2.8 ± 0.4	3.3 ± 0.4	3.0 ± 0.4

uncertainty of the integrated luminosity is 1% measured by analyzing events of the Bhabha scattering process [41]. The uncertainty related with the efficiencies of leptons, pions and photons is 1% for each particle [42,43]. The uncertainties related to the J/ψ mass window requirement and kinematic fit are estimated by tuning the MC sample for the J/ψ mass resolution and the helix parameters of charged tracks [44] according to data, and taking the resulting changes in efficiency as the uncertainties. The uncertainty associated with ISR correction factor is taken to be the difference of $(1 + \delta)^r \cdot \epsilon$ between the last two iterations in the cross section measurement. The uncertainties on the branching fractions of the intermediate states are taken from the PDG [1]. As described above, the signal yields are extracted by performing a simultaneous fit, thus, those uncertainties, which are correlated (i.e., luminosity, lepton and photon efficiencies), are directly propagated to the measured cross sections. Otherwise, we repeated the simultaneous fits by changing the corresponding value by $\pm 1\sigma$, individually, and the largest changes in the results are taken as the uncertainties. To extract the uncertainties associated with the fit procedure, we perform alternative fits by replacing the linear function with a second-order polynomial function for the background, fixing the width of the Gaussian function for the signal to be its nominal value and, in addition, changing its uncertainty and varying the fit range individually. The relative changes in the results are taken as the uncertainties. The efficiencies for the other selection criteria, the trigger simulation, the event start time determination, and the FSR simulation, exceed 99%, and their systematic errors are estimated to be less than 1%. Assuming all sources of uncertainties are independent, the total uncertainties in the $\eta J/\psi$ cross section measurement are determined to be 3.5%–13.7% depending on the c.m. energy. In general, the systematical errors are much smaller than the statistical ones. For details, we refer to Table III of the Supplemental Material [30].

To extract the resonant parameters of the structures observed in the measured cross sections, a simultaneous maximum-likelihood fit is performed to the results extracted from the XYZ and scan data. The fit function is a coherent sum of a P-wave phase space component (P-PHSP) [$\Phi(\sqrt{s})$] of the process $e^+e^- \rightarrow \eta J/\psi$ and three Breit-Wigner amplitudes ($B_{i=1,2,3}$) for the structures observed around 4040, 4230 and 4390 MeV/ c^2 , respectively:

$$\sigma^B(\sqrt{s}) = \left| C_0 \sqrt{\Phi(\sqrt{s})} + e^{i\phi_1} B_1(\sqrt{s}) + e^{i\phi_2} B_2(\sqrt{s}) + e^{i\phi_3} B_3(\sqrt{s}) \right|^2, \quad (2)$$

where ϕ_i is the relative phase of a resonance (i) to the P-PHSP component and C_0 is a free parameter. The parametrizations of the P-PHSP and Breit-Wigner components are given by

$$\Phi(\sqrt{s}) = \frac{q^3}{s}, \quad (3)$$

$$B_i(\sqrt{s}) = \frac{\sqrt{12\pi\mathcal{B}r_i\Gamma_i^{e^+e^-}\Gamma_i}}{s - M_i^2 + iM_i\Gamma_i} \sqrt{\frac{\Phi(\sqrt{s})}{\Phi(M_i)}}, \quad (4)$$

where q , M_i , Γ_i , $\Gamma_i^{e^+e^-}$ and $\mathcal{B}r_i$ are the daughter momentum in the rest frame of its parent, the mass, width, partial width of the decay in e^+e^- , and the branching fraction to $\eta J/\psi$ mode for the resonance i , respectively.

The fit is carried out by incorporating the statistical uncertainties only, where the number of events for the scan data are assumed to be Poisson distribution, and those for the XYZ data are Gaussian distribution [14]. Additionally, the beam energy spread of BEPCII (1.6 MeV) is considered by convolving with a Gaussian function whose width is 1.6 MeV [14,45]. The structure around 4040 MeV/ c^2 is assumed to be the $\psi(4040)$, and its mass and width are fixed to those given in the PDG [1], due to a lack of datasets at this energy region. Three solutions are found with equal fit quality and with identical masses and widths for the structures around 4220 and 4390 MeV/ c^2 . The fit quality is $\chi^2/\text{n.d.f.} = 107.7/120$, estimated by a χ^2 -test approach, where n.d.f. is the number of degrees of freedom. The fit results are summarized in Table I and the fit curves, according to solution 1, are exhibited in Fig. 2. It is noted that the second resonant structure has a mass of 4220 MeV/ c^2 , which is significantly higher than that of the $\psi(4160)$ observed in the same process by the Belle experiment [28]. An alternative fit has been carried out in which we replaced the second resonance with the PDG values of the $\psi(4160)$. The resulting fit gave a significantly worse $\chi^2/\text{n.d.f.} = 178.1/118$. In this case, the statistical significance of the $\psi(4160)$ is found to be 8.1σ less than that of $Y(4220)$. Furthermore, we performed a fit with extra $\psi(4160)$, $Y(4320)$ and $\psi(4415)$ with fixed resonant parameters taken from the PDG in combination with our nominal fit parameters. In this case, we find a very small statistical significance of 0.5σ for each extra resonance.

The systematic uncertainties of the resonant parameters of the structures at 4220 and 4390 MeV/ c^2 and of the product of $\mathcal{B}r_i$ and $\Gamma_i^{e^+e^-}$ are discussed as follows. The uncertainties associated with the measured cross section are estimated by incorporating the correlated and uncorrelated systematic uncertainties of measured Born cross section in the fit. The uncertainty associated with the c.m. energy (0.8 MeV) [12] is common for all data samples and propagates directly to the mass measurement. The uncertainty associated with the fit range is investigated by excluding the last energy point $\sqrt{s} = 4.60$ GeV in the fit. The uncertainty from the $\psi(4040)$ resonant parameters is studied by varying the parameters within its uncertainties. We performed the alternative fits with above scenarios

individually. The resulting differences are taken as the systematic uncertainties, and are summarized in Table IV of the Supplemental Material [30].

The structure at 4390 MeV/ c^2 is observed for the first time in the process $e^+e^- \rightarrow \eta J/\psi$, the corresponding significance is studied by performing an alternative fit without this structure included. The significance of 6.0σ is calculated from likelihood difference, taking into account the change in the number of degrees of freedom from the nominal fit and incorporating all the uncertainties discussed above.

In summary, we measured the Born cross sections of $e^+e^- \rightarrow \eta J/\psi$ for c.m. energy between 3.81 and 4.60 GeV by using data samples collected by the BESIII experiment. The measured cross sections are fitted by including three resonant structures and assuming the lowest lying one is the $\psi(4040)$. The masses and widths of the two resonances are found to be $(4218.6 \pm 3.8 \pm 2.5)$ and $(4382.0 \pm 13.3 \pm 1.7)$ MeV/ c^2 and the width $(82.0 \pm 5.7 \pm 0.4)$ and $(135.8 \pm 60.8 \pm 22.5)$ MeV, respectively, where first uncertainties are statistical and second ones systematic. It should be noted that we found a resonant structure with a mass around 4220 MeV/ c^2 that is significantly higher than the one (4160 MeV/ c^2) observed by the Belle experiment [28]. A comparison of masses versus widths for the structures in this measurement as well as those obtained from the processes $e^+e^- \rightarrow \pi^+\pi^- J/\psi$ [12], $\pi^+\pi^-\psi(3686)$ [13], $\pi^+\pi^-h_c$ [14], $\omega\chi_{c0}$ [15] and $\pi^+D^0D^{*-}$ [16] by the BESIII experiment are presented in Fig. 3. The measured resonant parameters of the two observed structures are consistent with or close to those of previous measurements, however, the intrinsic scenario for the difference on width is still unknown. Assuming that the two observed structures are the $Y(4220)$ and $Y(4390)$, our result contributes the first measurement of the mass, width, and branching fraction of the two Y states in the $\eta J/\psi$ final state. Furthermore, it is worth noting that the measured cross section is of the same order as the ones measured in $e^+e^- \rightarrow \pi^+\pi^- J/\psi$, $\pi^+\pi^-h_c$

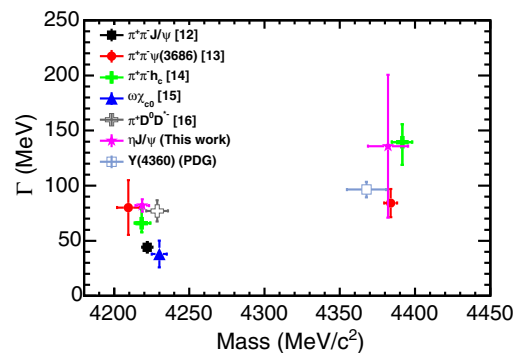


FIG. 3. Masses versus widths of the $Y(4220)$ and $Y(4390)$ obtained from the different final states by BESIII [46] and $Y(4360)$ quoted from PDG [1]. Here the errors reflect both statistical and systematic uncertainties.

and $\omega\chi_{c0}$. This observation may provide important information to eventually conclude on the nature of the Y states. Further theoretical developments including different scenarios of their internal structure are desirable.

ACKNOWLEDGMENTS

The BESIII Collaboration thanks the staff of BEPCII and the IHEP computing center and the supercomputing center of USTC for their strong support. This work is supported in part by National Key Basic Research Program of China under Contract No. 2015CB856700; National Natural Science Foundation of China (NSFC) under Contracts No. 11625523, No. 11635010, No. 11735014, No. 11822506, No. 11835012, No. 11935015, No. 11935016, No. 11935018, No. 11961141012, No. 11335008, No. 11375170, No. 11475164, No. 11475169, No. 11625523, No. 11605196, No. 11605198, No. 11705192; the Chinese Academy of Sciences (CAS) Large-Scale Scientific Facility Program;

Joint Large-Scale Scientific Facility Funds of the NSFC and CAS under Contracts No. U1732263, No. U1832207, No. U1532102, No. U1832103; CAS Key Research Program of Frontier Sciences under Contracts No. QYZDJ-SSW-SLH003, No. QYZDJ-SSW-SLH040; 100 Talents Program of CAS; INPAC and Shanghai Key Laboratory for Particle Physics and Cosmology; ERC under Contract No. 758462; German Research Foundation DFG under Contracts Nos. Collaborative Research Center CRC 1044, FOR 2359; Istituto Nazionale di Fisica Nucleare, Italy; Ministry of Development of Turkey under Contract No. DPT2006K-120470; National Science and Technology fund; STFC (United Kingdom); The Knut and Alice Wallenberg Foundation (Sweden) under Contract No. 2016.0157; The Royal Society, UK under Contracts No. DH140054, No. DH160214; The Swedish Research Council; U.S. Department of Energy under Contracts No. DE-FG02-05ER41374, No. DE-SC-0012069.

-
- [1] M. Tanabashi *et al.* (Particle Data Group), *Phys. Rev. D* **98**, 030001 (2018).
- [2] B. Aubert *et al.* (BABAR Collaboration), *Phys. Rev. Lett.* **95**, 142001 (2005).
- [3] C. Z. Yuan *et al.* (Belle Collaboration), *Phys. Rev. Lett.* **99**, 182004 (2007).
- [4] B. Aubert *et al.* (BABAR Collaboration), *Phys. Rev. Lett.* **98**, 212001 (2007).
- [5] X. L. Wang *et al.* (Belle Collaboration), *Phys. Rev. Lett.* **99**, 142002 (2007).
- [6] J. P. Lees *et al.* (BABAR Collaboration), *Phys. Rev. D* **89**, 111103 (2014).
- [7] X. L. Wang *et al.* (Belle Collaboration), *Phys. Rev. D* **91**, 112007 (2015).
- [8] J. P. Lees *et al.* (BABAR Collaboration), *Phys. Rev. D* **86**, 051102(R) (2012).
- [9] Z. Q. Liu *et al.* (Belle Collaboration), *Phys. Rev. Lett.* **110**, 252002 (2013).
- [10] T. E. Coan *et al.* (CLEO Collaboration), *Phys. Rev. Lett.* **96**, 162003 (2006).
- [11] M. Ablikim *et al.* (BESIII Collaboration), *Phys. Rev. Lett.* **114**, 092003 (2015).
- [12] M. Ablikim *et al.* (BESIII Collaboration), *Phys. Rev. Lett.* **118**, 092001 (2017).
- [13] M. Ablikim *et al.* (BESIII Collaboration), *Phys. Rev. D* **96**, 032004 (2017).
- [14] M. Ablikim *et al.* (BESIII Collaboration), *Phys. Rev. Lett.* **118**, 092002 (2017).
- [15] M. Ablikim *et al.* (BESIII Collaboration), *Phys. Rev. D* **99**, 091103 (2019).
- [16] M. Ablikim *et al.* (BESIII Collaboration), *Phys. Rev. Lett.* **122**, 102002 (2019).
- [17] H. X. Chen, W. Chen, X. Liu, and S. L. Zhu, *Phys. Rep.* **639**, 1 (2016).
- [18] N. Brambilla, S. Eidelman, C. Hanhart, A. Nefediev, C. P. Shen, C. E. Thomas, A. Vairo, and C. Z. Yuan, [arXiv: 1907.07583](https://arxiv.org/abs/1907.07583).
- [19] F. K. Guo, C. Hanhart, U. G. Meiner, Q. Wang, Q. Zhao, and B. S. Zou, *Rev. Mod. Phys.* **90**, 015004 (2018).
- [20] R. Lebed, R. Mitchell, and E. Swanson, *Prog. Part. Nucl. Phys.* **93**, 143 (2017).
- [21] S. L. Olsen, T. Skwarnicki, and D. Zieminska, *Rev. Mod. Phys.* **90**, 015003 (2018).
- [22] Y. P. Kuang, *Front. Phys. China* **1**, 19 (2006).
- [23] D. Y. Chen, X. Liu, and T. Matsuki, *Phys. Rev. D* **91**, 094023 (2015).
- [24] D. Y. Chen, C. J. Xiao, and J. He, *Phys. Rev. D* **96**, 054017 (2017).
- [25] M. N. Anwar, Y. Lu, and B. S. Zou, *Phys. Rev. D* **95**, 114031 (2017).
- [26] G. Li and X. H. Liu, *Phys. Rev. D* **88**, 094008 (2013).
- [27] Q. Wang, X. H. Liu, and Q. Zhao, *Phys. Rev. D* **84**, 014007 (2011).
- [28] X. L. Wang *et al.* (Belle Collaboration), *Phys. Rev. D* **87**, 051101 (2013).
- [29] M. Ablikim *et al.* (BESIII Collaboration), *Phys. Rev. D* **91**, 112005 (2015).
- [30] See Supplemental Material at <http://link.aps.org/supplemental/10.1103/PhysRevD.102.031101> for a summary of the number of signal events, luminosity, cross section, systematic uncertainty at each energy point and systematic uncertainty of fitted parameters.
- [31] M. Ablikim *et al.* (BESIII Collaboration), *Nucl. Instrum. Methods Phys. Res., Sect. A* **614**, 345 (2010).

- [32] S. Agostinelli *et al.* (GEANT4 Collaboration), *Nucl. Instrum. Methods Phys. Res., Sect. A* **506**, 250 (2003).
- [33] Z. Y. Deng *et al.* *Chin. Phys. C* **30**, 371 (2006).
- [34] D. Lange, *Nucl. Instrum. Methods Phys. Res., Sect. A* **462**, 152 (2001).
- [35] D. J. Lange, *Nucl. Instrum. Methods Phys. Res., Sect. A* **462**, 152 (2001).
- [36] S. Jadach, B. F. L. Ward, and Z. Was, *Comput. Phys. Commun.* **130**, 260 (2000); *Phys. Rev. D* **63**, 113009 (2001).
- [37] P. Golonka and Z. Was, *Eur. Phys. J. C* **45**, 97 (2006).
- [38] B. Andersson and H. Hu, arXiv:hep-ph/9910285.
- [39] S. Actis *et al.*, *Eur. Phys. J. C* **66**, 585 (2010).
- [40] E. A. Kuraev and V. S. Fadin, *Sov. J. Nucl. Phys.* **41**, 466 (1985).
- [41] M. Ablikim *et al.* (BESIII Collaboration), *Chin. Phys. C* **41**, 063001 (2017).
- [42] M. Ablikim *et al.* (BESIII Collaboration), *Phys. Rev. Lett.* **112**, 022001 (2014); *Phys. Rev. D* **83**, 112005 (2011).
- [43] M. Ablikim *et al.* (BESIII Collaboration), *Phys. Rev. D* **81**, 052005 (2010).
- [44] M. Ablikim *et al.* (BESIII Collaboration), *Phys. Rev. D* **87**, 012002 (2013).
- [45] E. V. Abakumova *et al.*, *Nucl. Instrum. Methods Phys. Res., Sect. A* **659**, 21 (2011).
- [46] For $\eta J/\psi$ process, the PHSP, $\psi(4040)$, $Y(4220)$ and $Y(4390)$ components are considered. For $\pi^+\pi^-J/\psi$ process, the exponential continuum, $\psi(3770)$, $Y(4220)$ and $Y(4230)$ components are considered. For $\pi^+\pi^-\psi(3686)$ process, the $Y(4220)$ and $Y(4390)$ components are considered. For $\pi^+\pi^-h_c$ process, the $Y(4220)$ and $Y(4390)$ components are considered. the $Y(4220)$ component is considered. For $\pi^+D^0D^{*-}$ process, The PHSP, $Y(4220)$ and $Y(4390)$ components are considered.